DERIVING MULTILAYERED MIXED-PHASE CLOUD PROPERTIES FROM RADAR AND LIDAR

JP1.4   Mahlon P. Rambukkange[1], Johannes Verlinde[1], Edwin W. Eloranta[2], Eugene E. Clothiaux[1], and Connor J. Flynn[3]

The Pennsylvania State University[1], The University of Wisconsin-Madison[2], Pacific Northwest National Laboratory[3]

1. INTRODUCTION

Mixed-phase clouds contain volumes composed of cloud droplets and ice crystals. Such a system is colloidally unstable and its complete theoretical understanding is lacking (Pinto 1998). Despite their colloidal instability, Arctic mixed phase clouds are observed to last anywhere from a few hours to days (Shupe et al. 2006). In the Arctic unlike at other latitudes, mixed-phase clouds occur at lower levels throughout the year (Intrieri et al. 2002b). Arctic clouds have a net radiative warming effect over the course of the year except for a short time in the summer (Curry 1993; Zhang 1996; Intrieri 2002a). Cloud droplets and ice crystals interact with radiation differently owing to dissimilarities in their particle sizes, shapes, concentrations and refractive indices. The delicate balance between the liquid and ice phases therefore plays a large role in determining mixed-phase cloud radiative properties. Accurate partitioning of the two-hydrometeor phases is crucial for accurately estimating the radiative fluxes at the Arctic surface.

Mixed-phase cloud characterization and hydrometeor phase separation with remote sensing instruments are challenging. Instruments such as cloud radars and lidars sense cloud geometrical boundaries differently because of their differing sensitivities to different parts of the particle size distribution. Dissimilar temporal and spatial resolutions of radars and lidars also create difficulties in comparing their data. Microwave radiometers have large angular beam widths compared to lidars and radars resulting in an even greater mismatch between their resolutions.

Although multilayered mixed-phase clouds are common in the Arctic, observational studies of these clouds are rare. At least part of the reason is that these multilayered clouds are difficult to observe even with multiple remote sensing instruments. For example, lidars have a high sensitivity to cloud droplets, but their signals are often completely attenuated by lower liquid layers. Even though Millimeter-Wavelength Cloud Radars (MMCR) can penetrate through several cloud layers, they are not sufficiently sensitive to detect tenuous liquid clouds. Microwave radiometer data are used to accurately retrieve liquid water path (LWP), but the LWP being an integral quantity does not provide information about the vertical distribution of the liquid water.

Rambukkange et al. 2010 demonstrate the use of MMCR Doppler spectra to separate cloud hydrometeor phase (i.e., liquid and ice) in multilayered mixed-phase clouds observed on October 6, 2004 during M-PACE. They utilized data from a collocated High Spectral Resolution Lidar (HSRL) to distinguish between liquid and ice. In this study, we employ their Doppler spectral phase partitions to compute contributions of liquid and ice to the radar reflectivity. After separating the HSRL backscatter into regions dominated by liquid and ice, we combine the radar and lidar data similar to Eloranta et al. (2007) to compute cloud microphysical properties of the ice and liquid. Finally, the performances of these retrievals are evaluated by testing them against properties derived only from the radar.

2. OVERVIEW OF THE DATA

Figure 1a shows the time-height cross section of the smallest hydrometeor velocity determined from individual Doppler spectra. Positive velocities correspond to downward motions. One can clearly identify regions with relatively strong downward motions by red and orange patches and others with near-zero velocities by yellow and green patches. Note that these yellow and green patches sometimes contain small regions with upward and downward motions.

[1] *Corresponding author address:* M. P. Rambukkange, Department of Meteorology, 503 Walker Building, University Park, PA 16802-5013 USA.
Phone: 814-865-1678; e-mail: mpr191@psu.edu.
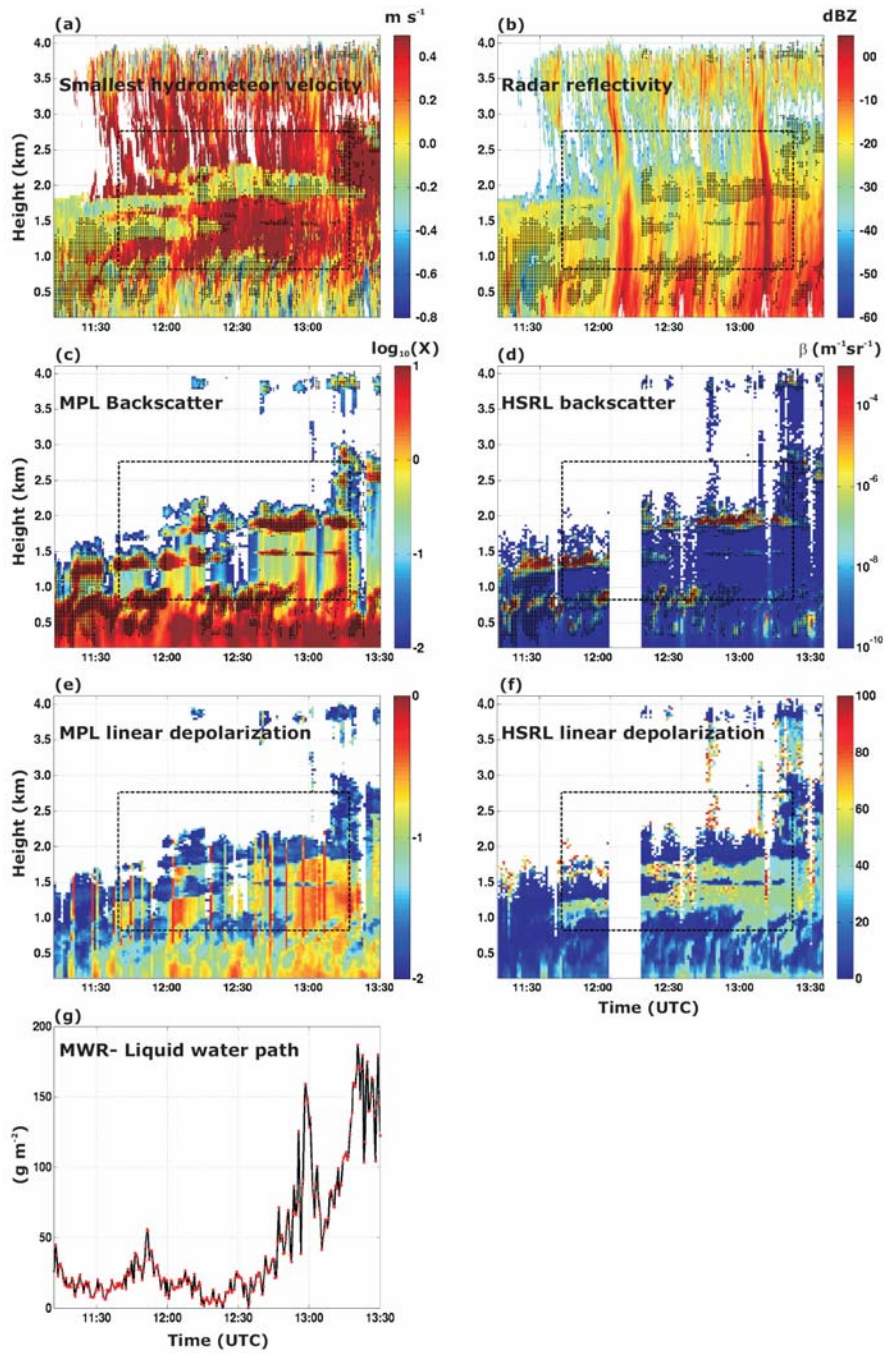
Fig.1. (a) Height versus time plot of the smallest hydrometeor velocity from Doppler spectra on October 6, 2004; (b) the radar reflectivity; (c) Micropulse Lidar (MPL) backscatter; (d) HSRL backscatter; (e) MPL linear depolarization and (f) HSRL linear depolarization. (g) The microwave radiometer derived LWP are shown by the red dots and the black line is the fit to the data. The region within the box is employed in this study. The black dots in (a)-(d) represent liquid regions determined from the HSRL.

Figure 1b displays the radar reflectivity. The radar detected clouds over the site up to an altitude of about 4 km. The strong vertical streaks in the reflectivity indicate individual precipitation events. Radar data alone cannot be employed in determining cloud hydrometeor phase, but it can be used to estimate cloud top. Depolarization lidars can be used to distinguish cloud phase and estimate the cloud base. Lidars can also measure cloud top when their signals are not completely attenuated within the cloud.

The attenuated backscatter from a Micropulse Lidar (MPL), collocated with the cloud radar, is plotted in Fig. 1c. The relatively strong backscatter values above 1 km suggest the presence of several cloud layers that are indistinguishable in the radar reflectivity. Since the MPL was not calibrated, it can only be used qualitatively. Therefore, we employ data from a collocated HSRL. The HSRL backscatter values (Fig. 1d) confirm the presence of multiple cloud layers over the site.

Figure 1e depicts the MPL linear depolarization. The comparison of Figs. 1c and 1e reveals that regions with high lidar backscatter are associated with low depolarization ratios. Therefore, regions with high backscatter contain liquid droplets. The HSRL linear depolarization in Fig. 1f shows similar features as the MPL depolarization. We employ the HSRL data to determine cloud volumes that contain liquid similar to Rambukkange et al. (2010). The black dots in Figs. 1a-d indicate cloud volumes that contain significant amounts of liquid. Note that these dots overlap with the green and yellow patches in Fig.1a; they overlap because the yellow-green layers in the smallest hydrometeor velocity are the signature of the liquid component. The LWP from the microwave radiometer in Fig. 1g also confirms the presence of liquid during this period.

3. MICROPHYSICAL RETRIEVALS

Eloranta et al. (2007) modified the method introduced by Donovan and van Lammeren (2001) to compute cloud microphysical properties with a radar and lidar. An underlying assumption with this method is that the radar and lidar data can be separated into regions dominated by ice and liquid based on applying thresholds to the lidar backscatters and depolarization ratios. After separating liquid and ice regions, the lidar and radar backscatter cross sections are used to compute particle mean and effective diameters, number density, water content for each phase. de Boer et al. (2009) applied this technique to multiple years of mixed-phase cloud data from the Arctic region. They discuss the possibility of large errors when dividing data into regions depending on the dominant phase rather than separating contributions from each phase within all cloud volumes.

In this study, we separate the radar reflectivity contributions from liquid and ice by independently integrating spectral reflectivities of each phase. Fig. 2a and 2b depict the radar reflectivity contributions of the ice and liquid. More details of partitioning the radar reflectivity according to the cloud hydrometeor phase are found in Rambukkange et al. (2010). Because of the unavailability of a method to separate the contributions of each phase in the lidar data, we divide the HSRL backscatter into regions dominated by liquid and ice. To prevent misidentifying regions we ensure that the data meet certain criteria on the circular depolarization ratios (δ_c) and backscatters (β). A pixel is identified as liquid if $\delta_c < 10\%$ and $\beta > 2.1 \times 10^{-6}$ (sr^{-1} m^{-1}), and ice when $\delta_c > 87\%$ and $\beta < 1 \times 10^{-6}$ (sr^{-1} m^{-1}). Data points that do not meet these requirement are discarded. Fig. 2c and 2d show the HSRL backscatters of liquid and ice regions. In these retrievals assuming an ice particle shape for ice regions below cloud is a large source of error (de Boer et al. 2009). We reduce this uncertainty by assuming an ice habit based on the temperature from the nearest sounding.

In addition to the radar-lidar method, we also employ a widely used radar-only method. One advantage of the radar-only method is that it can provide information about Arctic mixed-phase clouds under most conditions. The estimation of the ice water content (IWC) is based on an empirical relationship of the form $\mathrm{IWC} = aZ_e^b$, where a(=0.04) and b(=0.63) are fixed coefficients and Z_e is the radar reflectivity. The effective radii of ice crystals were computed with a power law relationship of a similar form $R_{ei} = aZ_e^b$ (a=54 and b=0.059). Both of these equations for the ice

phase have been derived for fall months at the North Slope of Alaska (Shupe et al. 2008).

Our radar-only retrieval of liquid cloud properties is also based on relationships between the radar reflectivity and cloud properties. The underlying assumption of the liquid retrieval is that the cloud droplet size distribution can be modeled with a lognormal distribution with a constant droplet number concentration (N_t) and logarithmic width (σ) with height. The relationships for droplet effective radius (R_{eff} in μm) and liquid water content (LWC, in g m^{-3}) takes the following forms:

$$R_{eff} = 50\left(\frac{Z_e}{N_t}\right)^{\frac{1}{6}} \exp\left(-0.5\sigma^2\right) \quad \text{and}$$

$$LWC = \rho_w\left(\frac{\pi}{6}\right)\left(\frac{Z_e}{N_t}\right)^{\frac{1}{2}} \exp\left(-4.5\sigma^2\right) \quad \text{(Frisch et al.}$$

1995, 2002). In the above equations relatively large changes in N_t or σ produces small changes in the effective radii, so we use N_t from M-PACE observations found in McFarquhar et al. (2007) and σ=0.31 (e.g., Frisch et al. 2002; Shupe et al. 2004, 2005).
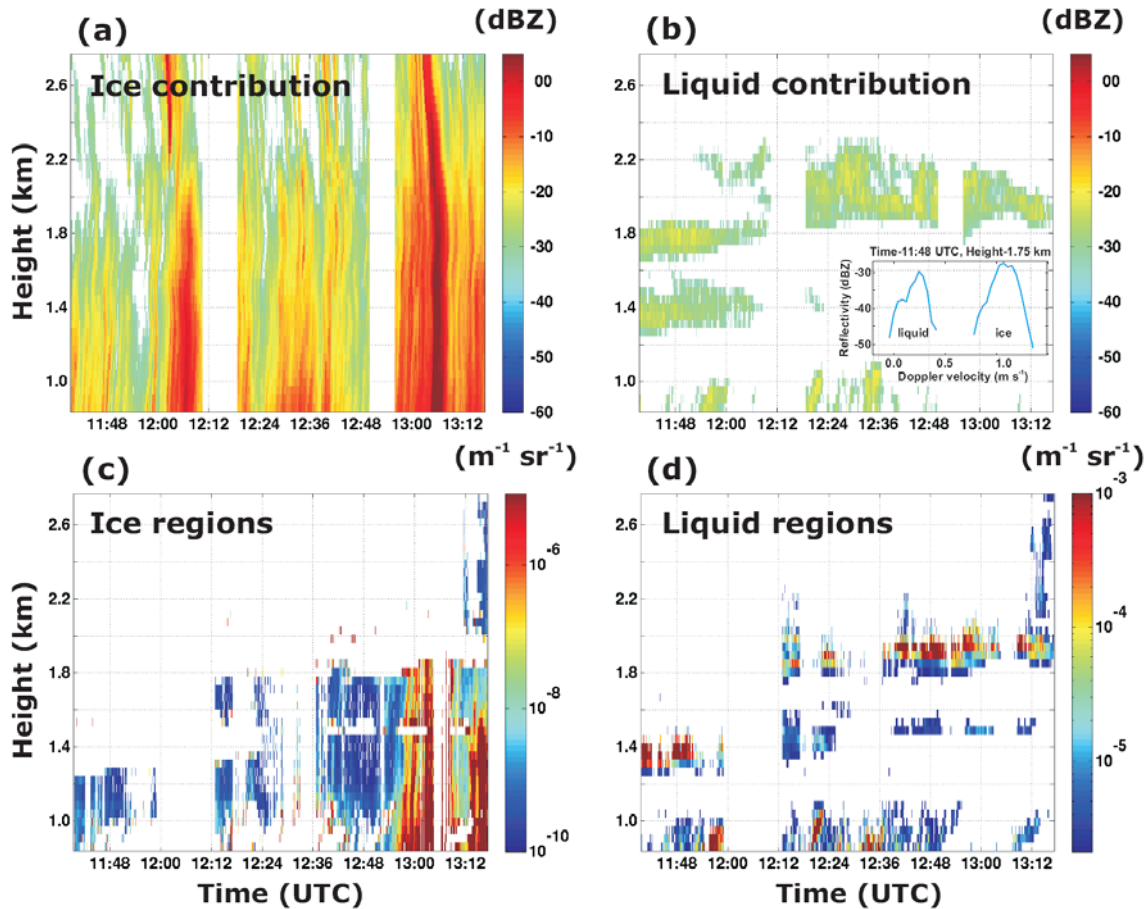
Fig. 2. The radar reflectivity contributions from (a) ice and (b) liquid. The HSRL backscatter separated into regions dominated by (c) ice and (d) liquid. Plotted on the top right is a Doppler spectrum clearly displaying well-separated liquid and ice peaks during the period.

4. RESULTS AND DISCUSSION

The performances of the radar-only and radar-lidar techniques are compared. In Fig. 3a the effective diameters from the radar-only method are plotted against those derived from the radar-lidar method. The effective diameters computed from the radar-lidar method span a larger range than those obtained from the radar-only method. With the exception of a small fraction of points many points lie close to the line with 45-degree slope. The plot of the LWCs estimated from the two techniques are displayed in Fig. 3b. In the radar only method LWC is proportional to $(Z_e)^{1/2}$, whereas the effective diameter is proportional to $(Z_e)^{1/6}$. Therefore, one would expect the LWCs obtained from the radar-only technique to shows greater variability than effective diameters from radar-only method. In Fig. 3b more points lie above the black-dashed line than below it, suggesting the possibility of a bias in the radar-only method.
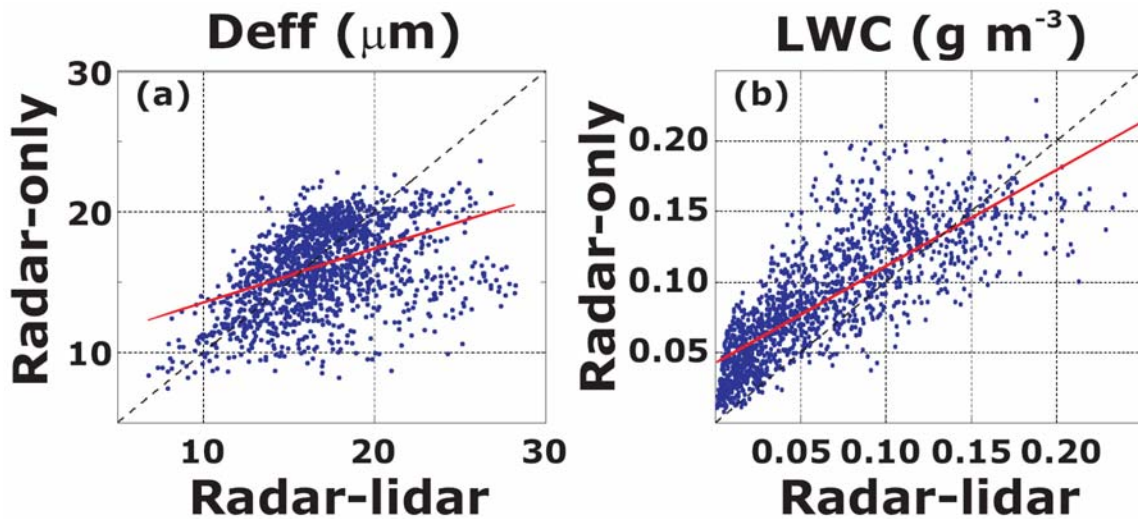
Fig.3. (a) Scatter plot of effective diameters for the liquid phase estimated from the radar-only and radar-lidar methods. (b) Scatter plot of LWCs estimated with both techniques. The quantities shown here are for the entire length of time.

Profiles of effective diameter, particle number concentration, and water content obtained from the radar-lidar method for the liquid and ice phase are displayed in Fig. 4. The liquid cloud microphysical profiles are plotted in red, while the ice phase profiles are plotted below cloud in blue. Ice profiles could not be obtained above the liquid cloud at 1.9 km because of complete attenuation of the lidar signals by the cloud. The lidar also detected a tenuous liquid cloud layer at 1.5 km, but the radar did not detect this liquid layer. Ice retrievals were hindered near this cloud because the lidar signals were dominated by the liquid phase.
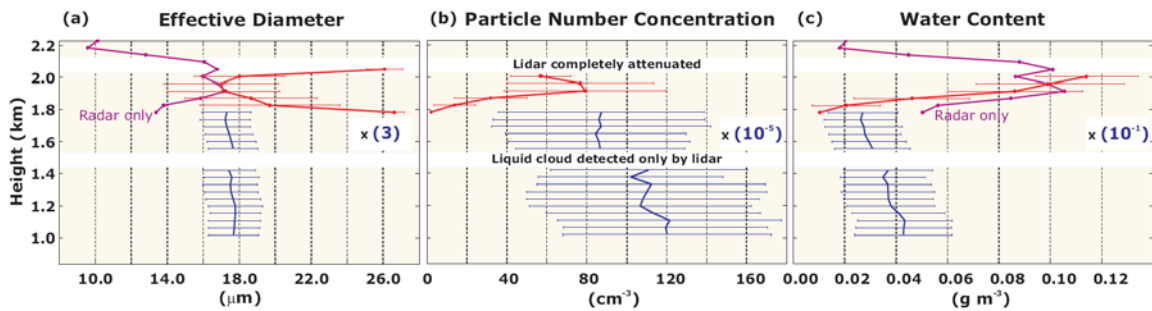
Fig.4. (a) Profiles of effective diameters of the liquid droplets (red) and ice particles (blue); (b) particle number concentrations; and (c) water contents. The horizontal lines show one standard deviation on both sides of the mean. The period used to compute these average profiles was 12:56-13:17 UTC. The constant factors used to scale the ice particles profiles values are given on the right side of each figure. The liquid properties from the radar-only method are plotted in purple.

The effective diameters of the liquid phase derived with the radar-only (purple) and radar-lidar (red) methods display similar values near the middle of the profile (see Fig.4a). These values in the middle are in good agreement with observations (M-PACE, McFarquhar et al. 2007). Despite this, the two profiles show completely opposite dependencies with height. Based on current theoretical understanding of stratus clouds one might select the profile derived only from radar data as the more realistic one.

The effective diameters of the ice crystals were estimated using hexagonal plates. The ice crystal effective diameters show less variability than those of cloud droplets at least partly because they were scaled to the range of droplets. The ice crystal effective diameters were also within the range of values observed during M-PACE.

Fig. 4b displays the radar-lidar particle number concentration of ice crystals and cloud droplets. Note that particle number concentrations cannot be directly retrieved from the radar data, hence is not shown in Fig. 4b. Similar to Arctic measurements (e.g., McFarquhar et al. 2007; de Boer et al. 2009) the liquid droplet concentrations are about four orders of magnitude greater than the ice crystal concentrations. However, stratus clouds droplet concentrations are usually constant with height above cloud base (Slingo et al. 1982; McFarquhar et al. 2007).

The water contents of ice and liquid particles as a function of height are shown in Fig. 4c. The radar-only and radar-lidar derived profiles demonstrate reasonable agreement between themselves and with M-PACE observations. Ice growth is implied by the increase in ice water content with decreasing height because the atmospheric layer between 0.5-2.4 km was supersaturated with respect to ice. The liquid water phase dominates the overall water mass in these mixed-phase clouds.

We examined the radar and lidar backscatter and their ratios, the main quantity used in the radar-lidar method, to answer questions regarding the unusual shape of some profiles of cloud droplets. Fig. 5 displays profiles of backscatter from the radar and lidar and their ratio. Both the radar and lidar backscatters increase above cloud base. The radar backscatter increases faster than the lidar backscatter with height because of the D^6 (radar) and D^2 (lidar) dependencies on the droplet diameter. However, at cloud base the radar backscatter is smaller than the lidar backscatter by about eight orders of magnitude. Therefore, lidar backscatter dominates the radar-lidar ratio throughout the cloud resulting in smaller backscatter ratios in the middle of the cloud and unrealistic profiles of effective diameters.
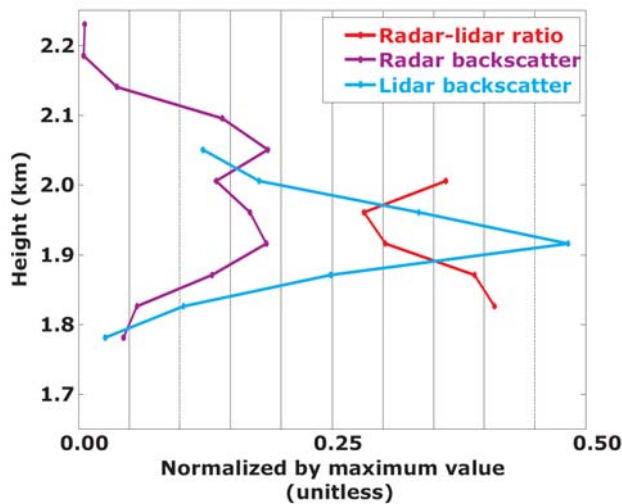
Fig.5. Lidar and radar backscatter profiles of liquid clouds are displayed in cyan and purple, respectively. Each profile has been normalized with respect to the maximum value in the domain. The radar-lidar backscatter ratio is plotted in red.

Another peculiar feature in the lidar data, but not in the radar data is that the lidar backscatter rapidly decreases after reaching its maximum value within cloud. We speculate that this drop in the lidar backscatter is due to attenuation of the lidar signal. When attenuation occurs, we no longer have a high confidence in the lidar data; therefore, we rejected portions of individual profiles at heights above which the lidar backscatter reaches it maximum value.

ACKNOWLEDGEMENTS

REFERENCES

Curry, J. A., J. L. Schramm, and E. E. Ebert, 1993: Impact of clouds on the surface radiation balance of the Arctic Ocean. *Meteorol. Atmos. Phys.*, **51**, 197–217.

de Boer, G., E. W. Eloranta, and M. D. Shupe, 2009: Arctic Mixed-Phase Stratiform Cloud Properties from Multiple Years of Surface-Based Measurements at Two High-Latitude Locations. *J. Atmos. Sci.* **66**, 2874-2887.

Donovan, D. P. and A. C. A. P. van Lammeren, 2001: Cloud effective particle size and water content profile retrievals using combined lidar and radar observations. 1. Theory and examples. *J. Geophys. Res.*, **106**, 27425–27448.

Eloranta, E. W., 2005: High Spectral Resolution Lidar, in Lidar: *Range-Resolved Optical Remote Sensing of the Atmosphere*, C. Weitkamp, Ed., Springer–Verlag, 143–163.

Eloranta E.W., T. Uttal and M. D. Shupe, 2007: Cloud particle size measurements in Arctic clouds using lidar and radar. Geoscience and Remote Sensing Symposium, 2007. IGARSS 2007. *IEEE International* 2265-2267.

Intrieri, J. M., C. F. Fairall, M. D. Shupe, O. G. P. Persson, E. L. Andreas, P. Guest, and R. M. Moritz, 2002a: An annual cycle of Arctic surface cloud forcing at SHEBA. *J. Geophys. Res.*,**107**, 8039, doi:10.1029/2000JC000439.

Intrieri, J. M., C. F. Fairall, M. D. Shupe, O. G. P. Persson, E. L. Andreas, P. Guest, and R. M. Moritz, 2002a: An annual cycle of Arctic surface cloud forcing at SHEBA. *J. Geophys. Res.*,**107**, 8039, doi:10.1029/2000JC000439.

Intrieri, J. M., M. D. Shupe, T. Uttal, and B. J. McCarty, 2002b: An annual cycle of Arctic cloud characteristics observed by radar and lidar at SHEBA. *J. Geophys. Res.*,**107**, 8030, doi:10.1029/2000JC000423.

McFarquhar, G. M., G. Zhang, M. R. Poellot, G. L. Kok, R. McCoy, T. Tooman, A. Fridlind, and A. J. Heymsfield, 2007: Ice properties of single-layer stratocumulus during the Mixed-Phase Arctic Cloud Experiment: 1. Observations. *J. Geophys. Res.*, 112:D24201. doi:10.1029/2007JD008633.

Pinto, J. O., 1998: Autumnal mixed-phase cloudy boundary layers in the Arctic. *J. Atmos. Sci.*, **55**, 2016–2038.

Rambukkange, M. P., J. Verlinde, E. W. Eloranta, C. J. Flynn, and E. E. Clothiaux, 2010: Using Doppler spectra to separate hydrometeor populations and analyze ice precipitation in multilayered mixed-phase clouds. *Geosci. Remote Sens. Lett., IEEE*, **99**, 108-112.

Sassen, K. 1984: Deep orographic cloud structure and composition derived from comprehensive remote sensing measurements. *J. Climate Appl. Meteor.*, **23**, 568–583.

Shupe, M.D., P. Kollias, S. Y. Matrosov, and T. L. Schneider, 2004: Deriving Mixed-Phase Cloud Properties from Doppler Radar Spectra. *J. Atmos. Oceanic. Technol.,* **21**, 660–670.

Shupe, M. D., T. Uttal, and S. Y. Matrosov, 2005: Arctic cloud microphysics retrievals from surface-based remote sensors at SHEBA. *J. Appl. Meteor.*, **44**, 1544–1562.

Shupe, M. D., S. Y. Matrosov, and T. Uttal, 2006: Arctic mixed-phase cloud properties derived from surface-based sensors at SHEBA. *J. Atmos. Sci.*, **63**, 697–711.

Shupe, M. D., P. Kollias, P. O. G. Persson, and G. M. McFarquhar, 2008: Vertical motions in Arctic mixed-phase stratiform clouds. *J. Atmos. Sci.*, **65**, 1304–1322.

Slingo, A., S. Nicholls, and J. Schmetz, 1982: Aircraft observations of marine stratocumulus during JASIN. *Quart. J. Roy. Meteor. Soc.*, **108**, 833–888.

Verlinde, J., Coauthors 2007: The Mixed-Phase Arctic Cloud Experiment. *Bull. Amer. Meteor. Soc.*, **88**, 205–221.

Zhang, T., K. Stamnes, and S. A. Bowling, 1996: Impact of clouds on surface radiative fluxes and snow melt in the Arctic and subarctic. *J. Climate*, **9**, 2110–2123.

Zuidema, P., Coauthors 2005: An Arctic springtime mixed-phase cloudy boundary layer observed during SHEBA. *J. Atmos. Sci.*, **62**,160–176.